
Revisiting Reweighted Risk for Calibration: AURC, Focal Loss, and Inverse Focal Loss

Han Zhou Sebastian G. Gruber Teodora Popordanoska Matthew B. Blaschko
 ESAT-PSI, KU Leuven, Belgium
 firstname.lastname@esat.kuleuven.be

Abstract

Several variants of reweighted risk functionals, such as focal loss, inverse focal loss, and the Area Under the Risk–Coverage Curve (AURC), have been proposed in the literature and claims have been made in relation to their calibration properties. However, focal loss and inverse focal loss propose vastly different weighting schemes. In this paper, we revisit a broad class of weighted risk functions commonly used in deep learning and establish a principled connection between these reweighting schemes and calibration errors. We show that minimizing calibration error is closely linked to the selective classification paradigm and demonstrate that optimizing a regularized variant of the AURC naturally leads to improved calibration. This regularized AURC shares a similar reweighting strategy with inverse focal loss, lending support to the idea that focal loss is less principled when calibration is a desired outcome. Direct AURC optimization offers greater flexibility through the choice of confidence score functions (CSFs). To enable gradient-based optimization, we introduce a differentiable formulation of the regularized AURC using the SoftRank technique. Empirical evaluations demonstrate that our AURC-based loss achieves competitive class-wise calibration performance across a range of datasets and model architectures.

1 Introduction

Over the past decade, advances in deep learning have enabled neural networks to achieve, and in some cases surpass, human-level performance on tasks ranging from image recognition [19] to natural language understanding [1, 33]. However, superior accuracy alone does not guarantee that the predicted confidence scores faithfully reflect true outcome probabilities – a phenomenon known as miscalibration [17]. Miscalibration can lead to critical errors in high-stakes applications where trustworthy uncertainty estimates are essential. To address and quantify this gap, the research community has introduced a range of calibration error metrics [5, 17, 30, 40] to evaluate the discrepancy between predicted confidences and observed outcome frequencies. Recent work has explored both trainable [4, 24, 26, 31, 40] and post-hoc [10, 17, 29, 36, 43] approaches for neural network calibration, achieving impressive reductions in terms of those calibration errors. Among trainable methods, focal loss [32]—which emphasizes hard examples during training—has gained popularity for its calibration benefits. Conversely, inverse focal loss [42], which focuses on the easy examples more, has also been shown to improve calibration in certain settings. This raises a key question: *Which weighting scheme is most effective for improving model calibration?*

We aim to answer this question by examining the relationship between selective classification [13] and calibration error. We provide a theoretical foundation that links calibration error minimization to the principles of selective classification. Building on this connection, we propose a loss function derived from the Area Under the Risk-Coverage Curve (AURC) [14], originally introduced in the context of selective classification, and demonstrate that it adopts a reweighting scheme similar to that

of the inverse focal loss. To enable gradient-based optimization, we leverage the SoftRank [3] method to approximate AURC in a differentiable manner. This adaptation ensures that our AURC-based loss remains differentiable with respect to any choice of confidence score function (CSF).

Our main **contributions** are summarized as follows:

- ① We establish a theoretical connection between calibration error minimization and selective classification by analyzing the structure of calibration error and its relation to the “abstain” strategy at the core of selective classification.
- ② Motivated by this connection, we propose a differentiable loss function based on the AURC metric. Although it adopts a reweighting strategy similar to that of inverse focal loss, it offers greater flexibility in the choice of CSFs.
- ③ We demonstrate through extensive experiments that our proposed AURC-based loss achieves competitive class-wise calibration performance across multiple datasets and network architectures, outperforming existing calibration-aware loss functions.

2 Related work

Post-hoc calibration methods address miscalibration by learning a mapping function that transforms model outputs into calibrated posterior probabilities. Approaches like Platt scaling [39], temperature scaling (TS) [17], and local temperature scaling [10] typically preserve classification accuracy by introducing a scalar temperature parameter. In contrast, other probabilistic methods—including Beta calibration [28], Dirichlet calibration [29], Gaussian processes [43], and the Concrete distribution [11]—may achieve better calibration but often at the cost of reduced classification accuracy. Notably, Dirichlet calibration generalizes Beta calibration to multi-class settings. Ma and Blaschko [36] and Liu et al. [35] proposed post-hoc calibration methods that adjust predicted probabilities based on correctness, using binary classifiers to either distinguish between correct and incorrect predictions or to directly modulate confidence accordingly. However, these approaches often involve a trade-off between calibration and predictive accuracy. We aim to develop a trainable calibration method that improves calibration performance without significantly compromising predictive accuracy.

Trainable calibration methods seek to enhance the calibration of deep neural networks by explicitly modifying the training objective. One class of approaches introduces differentiable surrogate losses that directly approximate the expected calibration error, as demonstrated in [4, 24, 26, 31, 40]. Popordanoska et al. [40] proposed ECE^{KDE}, a differentiable estimator of calibration error, and introduced the KDE-XE objective, which augments cross-entropy (XE) with an ECE-KDE regularizer to balance accuracy and calibration. Alternatively, several studies replace the standard cross-entropy loss with calibration-aware objectives, including mean squared error loss [23], inverse focal loss [42], and focal loss [32]. Focal loss, in particular, has been empirically shown to improve calibration by mitigating overconfident predictions [6, 25, 37]. Nevertheless, Wang et al. [42] argue that the regularization effect of focal loss may suppress important information about sample difficulty, thereby limiting the effectiveness of subsequent post-hoc calibration techniques. To address this trade-off, several variants of focal loss have been proposed, such as Adaptive Focal Loss [15] and Dual Focal Loss [41]. Distinct from these prior approaches, we propose a loss function based on the selective classification framework. While selective classification is not originally intended for calibration, we show that its underlying principle is fundamentally aligned with minimizing calibration error.

Selective classification augments a standard classifier with a reject option, enabling an explicit trade-off between selective risk and coverage. This technique mitigates selective risk by withholding low-confidence predictions [9, 12–14]. The Area Under the Risk-Coverage Curve (AURC) and its normalized variant, Excess-AURC (E-AURC) [14], are among the most widely used evaluation metrics for selective classification systems. These metrics compute the risk associated with accepted predictions across different confidence thresholds. Zhou et al. [46] showed that AURC can be interpreted as a weighted risk function, where the weights are determined by the ranking induced by a CSF g . This work is motivated by the goal of establishing a theoretical and empirical connection between selective classification and model calibration. We empirically show that minimizing a regularized AURC objective yields strong calibration performance across a range of architectures and datasets. While the underlying weighting scheme is similar to that of the inverse focal loss, our approach offers substantially greater flexibility in the choice of CSFs, making it more adaptable to different modeling scenarios.

3 Preliminaries

A common approach to training a classifier with a softmax output is to learn a function $f : \mathcal{X} \rightarrow \Delta^k$, which maps an input $\mathbf{x} \in \mathbb{R}^d$ to a probability distribution over k classes. The output $\mathbf{p} = f(\mathbf{x}) = (p_1, \dots, p_k)^\top \in \Delta^k$ is a vector in the probability simplex, representing the predicted class probabilities. Given an input \mathbf{x} , let $y' \in \{1, \dots, k\}$ denote the true class label, and define its one-hot encoded label $\mathbf{y} = (y_1, \dots, y_k)^\top \in \{0, 1\}^k$, where $y_{y'} = 1$ and $y_j = 0$ for all $j \neq y'$.

3.1 Weighted Risk Functions

To train the classifier f , one typically minimizes the expected loss over the joint probability distribution $\mathbb{P}(\mathbf{x}, \mathbf{y})$:

$$\mathcal{R}(f) = \mathbb{E}[\ell(\mathbf{p}, \mathbf{y})], \quad (1)$$

where ℓ is a loss function, such as cross-entropy or squared loss. These conventional loss functions treat all samples equally, which may not be optimal in scenarios with imbalanced data or varying prediction confidence. A widely adopted alternative is the focal loss, a weighted loss function that emphasizes uncertain or misclassified examples.

Definition 3.1 (Focal Loss). Let \mathbf{x} be an input vector, $\gamma \geq 0$ a focusing parameter, and f a model mapping from the feature space into the probability simplex. The focal loss is defined as:

$$\ell_{\text{FL}}(\mathbf{p}, \mathbf{y}) = -(1 - p_{y'})^\gamma \ln(p_{y'}), \quad (2)$$

where $p_{y'}$ denotes the predicted probability corresponding to the true class label y' .

Focal loss reduces to cross-entropy when $\gamma = 0$. More generally, it can be interpreted as a reweighted version of cross-entropy, where each instance is assigned an importance weight $\mathbf{w}(\mathbf{p}) = (1 - \mathbf{p})^\gamma \in \mathbb{R}^k$. The weight depends on both the predictive probability $p_{y'}$ and the focusing parameter γ : samples predicted with high confidence are downweighted, while harder or less confident samples are emphasized when $\gamma \geq 1$.

Definition 3.2 (Inverse Focal Loss). Let \mathbf{x} be an input vector, $\gamma \geq 0$, and f a model mapping into the probability simplex. The inverse focal loss is defined as:

$$\ell_{\text{IFL}}(\mathbf{p}, \mathbf{y}) = -(1 + p_{y'})^\gamma \ln(p_{y'}), \quad (3)$$

where $p_{y'}$ denotes the predicted probability for the true class label y' .

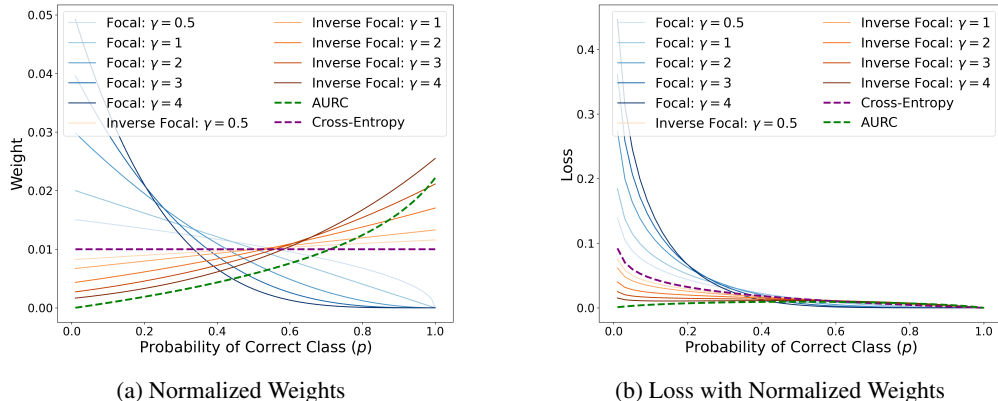


Figure 1: Comparison of weight and loss behavior with respect to prediction probability p . We normalize the weights in both focal loss and inverse focal loss for fair comparison.

In contrast to focal loss, which downweights confident predictions, inverse focal loss assigns greater weight to high-confidence samples. We analytically derive the gradient of inverse focal loss (App. 7.3) and show empirically that certain values of γ may lead to undesirable behavior during training (see Fig. 5 in appendix). Surprisingly, despite their fundamentally opposite reweighting schemes, both strategies have been reported to improve classifier calibration.

3.2 Selective classification

Selective classification pairs a classifier f with a *confidence scoring function* $g : \mathcal{X} \rightarrow [0, 1]$, which estimates the reliability of its predictions. A selective classifier, defined as the pair (f, g) , makes a prediction only when the confidence score exceeds a threshold $\tau \in \mathbb{R}$, and abstains otherwise:

$$(f, g)(\mathbf{x}) := \begin{cases} f(\mathbf{x}) & \text{if } g(\mathbf{x}) \geq \tau, \\ \text{"abstain"} & \text{otherwise.} \end{cases} \quad (4)$$

The selective risk w.r.t. the data distribution $\mathbb{P}(\mathbf{x}, \mathbf{y})$ is defined as:

$$R(f, g) := \frac{\mathbb{E}[\ell(f(\mathbf{x}), \mathbf{y}) \cdot \mathbb{I}(g(\mathbf{x}) \geq \tau)]}{\mathbb{E}[\mathbb{I}(g(\mathbf{x}) \geq \tau)]}. \quad (5)$$

where \mathbb{I} is the indicator function and the denominator represents the *Coverage*. The threshold τ determines the trade-off between selective risk and coverage. Rather than evaluating performance at a single threshold, the AURC [14] assesses classifier robustness across all possible thresholds, as induced by the distribution of confidence scores. This metric can equivalently be expressed as a weighted risk function [46], as described below.

Definition 3.3 (AURC). Let $\mathbf{p} = f(\mathbf{x})$ be the predicted probability vector produced by the model. The cumulative distribution function (CDF) of the CSF $g(\mathbf{p})$ is defined as:

$$G(\mathbf{p}) = \Pr(g(\mathbf{p}') \leq g(\mathbf{p})) = \int \mathbb{I}[g(\mathbf{p}') \leq g(\mathbf{p})] d\mathbb{P}(g(\mathbf{p}')). \quad (6)$$

Then, the AURC metric is given by:

$$\text{AURC}_g(f) = -\mathbb{E}[\ln(1 - G(\mathbf{p})) \cdot \ell(\mathbf{p}, \mathbf{y})]. \quad (7)$$

This formulation reveals that AURC can be interpreted as a reweighted risk, where each sample is weighted by $w(\mathbf{p}) = -\ln(1 - G(\mathbf{p}))$, a function that depends on the CSF. Common choices for the CSFs include the Maximum Softmax Probability (MSP), i.e., $g(\mathbf{p}) = \max_{i=1}^k p_i$, or the entropy of the logits prior to the softmax layer.

3.3 Calibration Errors

Below, we provide the definitions of commonly used calibration errors and their empirical estimators.

Definition 3.4 (Calibrated). A model $f : \mathcal{X} \rightarrow \Delta^k$ is *calibrated* if and only if $f(\mathbf{x}) = \mathbb{E}[\mathbf{y} \mid f(\mathbf{x})]$.

Definition 3.5 (L_ρ Calibration Error (CE_ρ)). The L_ρ calibration error of a model $f : \mathcal{X} \rightarrow \Delta^k$, with $\rho \geq 1$, is defined as:

$$\text{CE}_\rho(f) = (\mathbb{E}[\|f(\mathbf{x}) - \mathbb{E}[\mathbf{y} \mid f(\mathbf{x})]\|_\rho^\rho])^{1/\rho}, \quad (8)$$

where the expectation is taken with respect to $\mathbb{P}(\mathbf{x}, \mathbf{y})$.

When $\rho = 1$, this quantity is referred to as the *Expected Calibration Error (ECE)* [17]. In practice, the true value of $\text{CE}_\rho(\cdot)$ is unobservable, as it depends on the unknown joint distribution $\mathbb{P}(\mathbf{x}, \mathbf{y})$. To address this, Guo et al. [17] proposed an empirical estimator based on a finite dataset. This estimator employs a binning scheme B to approximate the true difference between the predicted confidence and the conditional probability $\mathbb{E}[\mathbf{y} \mid f(\mathbf{x})]$ by computing empirical averages within each bin. We denote this estimator as $\widehat{\text{ECE}}_B$.

Definition 3.6 (Binned estimator $\widehat{\text{ECE}}_B$). Let the binning scheme be $B = \{I_b \mid b = 1, \dots, m\}$, the binned estimator is denoted as:

$$\widehat{\text{ECE}}_B(f) = \sum_{b=1}^m \frac{n_b}{n} |\text{acc}_b(f) - \text{conf}_b(f)| \quad (9)$$

where n_b is the number of samples falling into bin I_b , n is the total number of samples, $\text{conf}_b(f)$ is the average predicted confidence in bin I_b , and $\text{acc}_b(f)$ is the accuracy in that bin.

To avoid potential confusion, we emphasize here the empirical estimator of ECE measures the top-label calibration error instead of the calibration error w.r.t. a fixed class. The *class-wise calibration error (cwECE)* [30] measures the expected calibration errors across all classes.

Definition 3.7 (Class-Wise Calibration Error (cwECE $_{\rho}$)). The class-wise calibration error is:

$$\text{cwECE}_{\rho}(f) = \frac{1}{k} \left(\sum_{c=1}^k \mathbb{E} [|f_c(\mathbf{x}) - \mathbb{P}(y' = c | f_c(\mathbf{x}))|^{\rho}] \right)^{1/\rho}, \quad (10)$$

for $1 \leq \rho \in \mathbb{R}$, where $f_c(\mathbf{x})$ is the predicted probability for class c , and y' is the true class label.

We follow related works [18, 38] in defining this metric as the average calibration error across classes. Similar to ECE, it can be estimated empirically using a binning scheme B , resulting in a bin-based estimator $\widehat{\text{cwECE}}_B(f)$.

Definition 3.8 (Binned estimator $\widehat{\text{cwECE}}_B$). Let m_c be the number of bins for class c and the binning scheme be $B = \{I_{c,b} | c = 1, \dots, k; b = 1, \dots, m_c\}$, The binned estimator for $\rho = 1$ is given by:

$$\widehat{\text{cwECE}}_B(f) = \frac{1}{k} \sum_{c=1}^k \frac{1}{n} \sum_{b=1}^{m_c} n_{c,b} \left| \underbrace{\frac{1}{n_{c,b}} \sum_{i \in I_{c,b}} \mathbb{I}(y'_i = c)}_{\text{acc}_{c,b}} - \underbrace{\frac{1}{n_{c,b}} \sum_{i \in I_{c,b}} f_c(\mathbf{x}_i)}_{\text{conf}_{c,b}} \right| \quad (11)$$

where $n_{c,b}$ is the number of samples in bin $I_{c,b}$, and n is the total number of samples.

4 A Differentiable Loss Function Derived from Selective Classification

In this section, we begin by examining lower bounds for two widely used calibration metrics—ECE and class-wise ECE—as presented in Prop. 4.1–4.3. These results provide theoretical insight into how calibration error can be reduced for a pre-trained model and motivate a deeper exploration of the connection between selective classification and calibration. Building on these insights, we propose a differentiable loss function derived from the AURC metric in selective classification. The formulation is fully differentiable—enabled by the SoftRank method—and supports arbitrary CSFs.

4.1 Linking Calibration Error Minimization to Selective Classification

Lemma 4.1 (Lower bound of ECE [36, Prop. 2]). *Let $f : \mathcal{X} \rightarrow \Delta^k$ be the classifier and $\widehat{\text{err}}(f)$ be its empirical error rate on a finite set $\{(\mathbf{x}_i, y_i)\}_{i=1}^n$ given by $\widehat{\text{err}}(f) = \frac{1}{n} \sum_{i=1}^n \mathbb{I}(\hat{y}_i \neq y'_i)$ where $\hat{y}_i = \arg \max_{c \in [k]} f_c(x_i)$. For the top-label ECE computed over all binning schemes $B \in \mathcal{B}$,*

$$\text{ECE}(f) \geq \sup_{B \in \mathcal{B}} \widehat{\text{ECE}}_B(f) \geq \frac{\widehat{\text{err}}(f)}{k}. \quad (12)$$

In the proof of Prop. 4.1, Ma and Blaschko [36] demonstrate that a calibrated model can be constructed using a binary classifier that separates correct from incorrect predictions. We reinterpret this insight through the lens of selective classification, yielding the following result.

Proposition 4.2 (Optimal Calibration Map for ECE [36, Prop. 3]). *Suppose we are given a CSF g that perfectly distinguishes correct from incorrect predictions via a threshold τ , and a model $f : \mathcal{X} \rightarrow \Delta^k$. Then, we can construct a modified model f' such that:*

$$\sup_{B \in \mathcal{B}} \widehat{\text{ECE}}_B(f') \leq \sup_{B \in \mathcal{B}} \widehat{\text{ECE}}_B(f), \quad (13)$$

with the following adjustment:

$$\max_c f'_c(\mathbf{x}) = \begin{cases} 1 & \text{if } g(\mathbf{x}) \geq \tau, \\ \frac{1}{k} & \text{if } g(\mathbf{x}) < \tau. \end{cases} \quad (14)$$

Apart from this modification, f' is identical to f .

This proposition suggests that ECE can be improved by boosting the predicted confidence for correctly classified samples while reducing it for incorrect ones. Notably, assigning a uniform prediction $\frac{1}{k}$ when $g(\mathbf{x}) < \tau$ mimics the abstention mechanism used in selective classification. In this context, the CSF with a threshold τ effectively acts as a binary classifier. To further support the connection between calibration errors and selective classification, we next extend Prop. 4.1 to the cwECE and derive a constructive rule for minimizing it.

Proposition 4.3 (Lower Bound of cwECE). *For any class-wise binning scheme $B \in \mathcal{B}$, the class-wise ECE satisfies the lower bound:*

$$\text{cwECE}(f) \geq \sup_{B \in \mathcal{B}} \widehat{\text{cwECE}}_B(f) > \frac{1}{k} \widehat{\text{err}}(f). \quad (15)$$

The proof is provided in App. 7.2, and we sketch it here. First, we apply Minkowski's inequality to derive a lower bound on the supremum over all class-wise binning schemes. Next, we show that this supremum is bounded below by $\widehat{\text{err}}(f)/k$, unless f is perfectly accurate. Finally, by invoking Jensen's inequality, as in Kumar et al. [30], the lower bound follows. This construction naturally leads to a procedure for improving cwECE, analogous to Prop. 4.2.

Proposition 4.4 (Optimal Calibration Map for cwECE). *Let g be a CSF that perfectly separates correct and incorrect predictions via threshold τ , and let $f : \mathcal{X} \rightarrow \Delta^k$. Then a modified model f' can be constructed such that:*

$$\sup_{B \in \mathcal{B}} \widehat{\text{cwECE}}_B(f') \leq \sup_{B \in \mathcal{B}} \widehat{\text{cwECE}}_B(f), \quad (16)$$

with:

$$\max_c f'_c(\mathbf{x}) = \begin{cases} 1 & \text{if } g(\mathbf{x}) \geq \tau, \\ \min\left(\frac{1}{2}, \max_c f_c(\mathbf{x})\right) & \text{otherwise.} \end{cases} \quad (17)$$

All other components of f' are the same as in f .

This construction rule follows directly from the proof of Prop. 4.3. While slightly different from Prop. 4.2, this result similarly suggests that reducing the maximum predicted probability for uncertain samples helps improve cwECE. Together, these propositions build a theoretical foundation connecting selective classification with calibration error minimization: while Prop. 4.2 addresses ECE, Prop. 4.3 and its constructive variant extend this idea to cwECE. We conclude by presenting a result from Gruber and Buettnner [16], which synthesizes calibration metrics under a unified theoretical bound.

Proposition 4.5 (Hierarchy Among Calibration Metrics [16, Theorem 3.1]). *Let $f : \mathcal{X} \rightarrow \Delta^k$ be a classifier, and let $1 \leq \rho \leq 2$. Then:*

$$n^{\frac{1}{\rho} - \frac{1}{2}} \sqrt{BS(f)} \geq CE_\rho(f) \geq \begin{cases} k \cdot \text{cwECE}_\rho(f), & \geq 0, \\ \text{ECE}(f), & \end{cases} \quad (18)$$

where BS denotes the Brier score.

The proposition formalizes a hierarchy of calibration metrics, showing that L_ρ calibration error is upper bounded by a scaled Brier score and lower bounded by both cwECE and ECE. Thus, minimizing ECE or cwECE serves as a practical proxy for improving overall calibration performance.

4.2 Regularized AURC Loss Function

Given the preceding results, reducing calibration error requires lowering the maximum predicted probability for low-confidence samples—a strategy that echoes the "abstain" mechanism central to selective classification. Since the AURC metric originates from the selective classification framework and employs a weighting scheme similar to that of inverse focal loss (see Fig. 1), such reweighting schemes are theoretically well-suited for calibration error minimization. Motivated by this, we propose the *regularized AURC* (r-AURC) loss to examine whether this reweighting approach can effectively enhance model calibration. An asymptotically unbiased Monte Carlo estimator [46] for the population AURC defined in Eq. (7) is given by:

$$\widehat{\text{AURC}}_g(f) = -\frac{1}{n} \sum_{i=1}^n \ln \left(1 - \frac{r_i}{n+1} \right) \ell(\mathbf{p}_i, \mathbf{y}_i), \quad (19)$$

where $r_i := r(g(\mathbf{p}_i))$ denotes the rank of the confidence score $g(\mathbf{p}_i)$ among all samples in ascending order. Thus, a larger r_i corresponds to a higher confidence. This estimator is consistent and can be directly used as a training loss to minimize the AURC metric. Importantly, since $r_i = r(g(\mathbf{p}_i))$ is a function of the model output \mathbf{p}_i , its gradient $\frac{\partial r_i}{\partial \mathbf{p}_i}$ must be considered in backpropagation. To facilitate end-to-end optimization, we adopt the *SoftRank* approximation [3], which replaces the hard (non-differentiable) rank with a smooth, differentiable surrogate \hat{r}_i . This enables standard gradient-based training, as outlined in Algorithm 1.

Algorithm 1 AURC Optimization with SoftRank

Require: Training batch $\{(\mathbf{x}_i, \mathbf{y}_i)\}_{i=1}^n$, model f_θ , a CSF $g(\cdot)$, learning rate η

Ensure: Update: $\theta \leftarrow \theta - \eta \nabla_\theta L$

- 1: **Forward Pass:**
- 2: $\mathbf{p}_i \leftarrow f_\theta(\mathbf{x}_i)$ ▷ Model prediction
- 3: $\hat{r}_i \leftarrow \text{SoftRank}(g(\mathbf{p}_i))$
- 4: $L \leftarrow \frac{1}{n} \sum_{i=1}^n [-\ln(1 - \hat{r}_i) \cdot \ell(\mathbf{p}_i, \mathbf{y}_i)]$ ▷ AURC loss
- 5: **Backward Pass:**
- 6: **for** each $(\mathbf{x}_i, \mathbf{y}_i)$ in batch **do**
- 7: Compute $\nabla_{\mathbf{p}_i} L$ via Eq. (40)
- 8: $\nabla_\theta L += (\nabla_{\mathbf{p}_i} L)^\top \nabla_\theta \mathbf{p}_i$
- 9: **end for**

This loss function typically relies on sorting based on the confidence score function (CSF), incurring a computational cost of $\mathcal{O}(n \log(n))$ computation cost, which is generally more efficient than kernel-based calibration error losses that require quadratic time. To better understand the effect of CSF on AURC metric, we define the perfectly aligned CSF.

Definition 4.6 (Perfectly Aligned CSF). A CSF g^* is said to be *perfectly aligned* with the loss function ℓ if, for any two predictions $\mathbf{p}_i, \mathbf{p}_j$ with corresponding labels $\mathbf{y}_i, \mathbf{y}_j$, the following holds:

$$g^*(\mathbf{p}_i) \leq g^*(\mathbf{p}_j) \Rightarrow \ell(\mathbf{p}_i, \mathbf{y}_i) \geq \ell(\mathbf{p}_j, \mathbf{y}_j). \quad (20)$$

This condition ensures that higher confidence scores correspond to lower losses, meaning that the confidence ranking is consistent with the loss. In practice, this alignment significantly affects the effectiveness of the r-AURC loss, as it governs how the sample weights (via soft rank) interact with the loss values.

Proposition 4.7 (Lower Bound for Empirical AURC). *Let g^* be a CSF that is perfectly aligned with the loss function ℓ . Let \mathcal{G} denote the set of all valid confidence mappings. For a given model f and the cross-entropy loss, the empirical AURC is minimized at g^* , and has the following lower bound:*

$$\inf_{g \in \mathcal{G}} \widehat{\text{AURC}}_g(f) = \widehat{\text{AURC}}_{g^*}(f) \geq \frac{n \log 2}{2(n+1)} \widehat{\text{err}}^2(f) + \frac{\log 2}{2(n+1)} \widehat{\text{err}}(f), \quad (21)$$

where $\widehat{\text{err}}(f)$ is the empirical error of f on a finite dataset.

See App. 7.2 for the proof. This proposition indicates that AURC is minimized when the CSFs are perfectly aligned with the loss and when the model achieves high predictive accuracy. In addition, Prop. 4.1 and 4.3 show that lower calibration error also relies on the model being accurate. These insights collectively suggest that both calibration and accuracy are mutually reinforcing goals.

To this end, we consider the following constrained optimization framework to learn a model f that is both accurate and well-calibrated: $f = \arg \min_{f \in \mathcal{F}} \mathcal{R}(f)$, subject to $\text{AURC}_g(f) \leq B$, where $\mathcal{R}(f)$ denotes the expected predictive risk, and $B > 0$ is a user-defined budget. The corresponding Lagrangian relaxation of this constrained objective is given by:

$$f = \arg \min_{f \in \mathcal{F}} ((1 - \lambda) \mathcal{R}(f) + \lambda \text{AURC}_g(f)), \quad (22)$$

where $\lambda \in [0, 1]$ controls the trade-off between accuracy and AURC minimization. Note that the behavior of this regularized loss depends on the choice of the CSF g used in the AURC. As we show in later sections, different CSFs may lead to different calibration-performance.

Table 1: Test accuracy (%) and classwise ECE^a (↓), reported as mean $\times 10^2$ over 5 seeds.

Model	Accuracy (%) ↑						cwECE ^a (↓)					
	XE	FL-53	Inv.FL	r-A _p	r-A _e	r-A _m	XE	FL-53	Inv.FL	r-A _p	r-A _e	r-A _m
CIFAR-10												
ResNet50	94.75	94.43	95.00	94.61	94.30	94.63	0.266	0.591	0.287	0.260	0.249	0.259
ResNet110	94.56	94.32	95.05	94.44	94.25	94.53	0.275	0.544	0.294	0.264	0.271	0.269
WRN	95.30	94.03	95.42	95.42	95.17	95.56	0.236	1.059	0.256	0.251	0.244	0.220
PreResNet56	93.39	93.05	93.78	93.36	93.22	93.38	0.308	0.592	0.383	0.324	0.323	0.313
CIFAR-100												
ResNet50	77.54	68.08	77.92	77.68	76.30	77.62	0.092	0.239	0.100	0.091	0.091	0.091
ResNet110	77.21	71.13	77.32	77.43	71.87	77.49	0.098	0.178	0.111	0.097	0.131	0.095
WRN	78.68	72.68	78.73	78.73	78.66	78.86	0.094	0.190	0.106	0.092	0.094	0.098
PreResNet56	72.21	66.06	72.63	72.43	72.53	72.34	0.107	0.192	0.113	0.105	0.090	0.106
Tiny-ImageNet												
ResNet50	81.84	78.24	79.56	82.11	82.47	82.31	0.126	0.177	0.136	0.127	0.122	0.123

5 Experiments

Datasets and Models. We conduct experiments on image classification datasets including CIFAR-10, CIFAR-100 [27], and Tiny-ImageNet [8]. For Tiny-ImageNet, all images are resized to 224×224 pixels. On CIFAR-10/100, we evaluate models including WideResNet-28x10 [45], PreResNet-56 [21], and ResNet architectures with depths 50 and 110 [20]. For Tiny-ImageNet, we use pre-trained models from the *timm* library [44]. Each experiment is repeated with five different random seeds, and we report the mean of the resulting performance metrics.

r-AURC loss. For the regularized AURC objective (r-AURC) defined in Eq. (22), we set the trade-off parameter $\lambda = 0.5$ for all datasets. The regularization parameter ε is set to 0.05 for CIFAR-10 and 0.01 for CIFAR-100 and Tiny-ImageNet. Detailed selection for ε and λ is provided in App. 7.6. To thoroughly evaluate the r-AURC loss, examine its performance under different CSFs, including the Maximum Softmax Probability (MSP) [22], Negative Entropy [34], and Softmax Margin [2], as outlined in Table 3. We denote the corresponding variants as as r-A_p, r-A_e, and r-A_m, respectively.

Evaluation Metrics. We evaluate calibration performance using the binned estimators of ECE and class-wise ECE (cwECE), computed under two binning strategies: equal-width binning (denoted as ECE and cwECE) and adaptive binning [9] (denoted as ECE^a and cwECE^a). In addition, we consider a kernel density estimation-based calibration error, denoted as ECE^{KDE} [40], which provides a continuous, non-binned alternative. To assess whether our proposed r-AURC loss directly improves its intended objective, we also report the AURC metric in all evaluations.

Baselines. We explore the trainable calibration methods including cross-entropy loss (XE), KDE-XE [40], focal loss [37], inverse focal loss [42], and dual focal loss [41]. For focal loss, we consider FL-53 where $\gamma = 5$ for $f_{y'}(\mathbf{x}) \in [0, 0.2)$ and $\gamma = 3$ otherwise. For the latter two loss functions, the γ parameter is fine-tuned on the split validation set following the settings in Tao et al. [41]. For inverse focal loss, we note that when $\gamma > 3.5$, it may not able to update the model properly due to the positive gradients, as detailed discussed in App. 7.3. For KDE-XE, we set its regularization parameter $\lambda = 0.3$ on CIFAR-10, and $\lambda = 0.5$ on CIFAR-100, to achieve the best canonical calibration error as suggested in the original paper. We also evaluate post-hoc calibration methods, such as *MetaAcc* [36] and Temperature Scaling (TS) [17], on models trained with different loss functions. (See App. 7.5 for additional results on those baselines.)

Results. Table 1 presents the test performance in terms of cwECE across different loss functions. Overall, the proposed r-AURC loss consistently outperforms other baselines, while focal loss tends to yield the worst cwECE in most cases. Notably, the performance of r-AURC is sensitive to the choice of CSF; for instance, MSP proves suboptimal on CIFAR-10, underscoring the importance of selecting a suitable CSF to ensure reliable calibration. In Fig. 2, focal loss tends to be overconfident on easy samples, whereas AURC-based losses exhibit better-calibrated behavior. As shown in Table 2, the cwECE^a of r-AURC can be further reduced via TS, highlighting the benefit of post-hoc calibration. Additional results in Appendix 7.5 show that *MetaAcc* can further enhance cwECE—particularly for losses other than focal loss—though this often comes at the cost of reduced predictive accuracy.

Table 2: Mean cwECE $\times 10^2$ (\downarrow) before and after TS. The temperature T selected by minimizing the ECE on the training set is shown in brackets next to each TS result.

Model	XE	FL-53	Inv. FL	r-A _p	r-A _e	r-A _m
CIFAR-10						
ResNet50	0.641	0.838	0.805	0.629	0.621	0.644
+TS	0.456 [1.30]	0.911 [1.02]	0.692 [1.36]	0.438 [1.29]	0.407 [1.28]	0.457 [1.30]
ResNet110	0.670	0.767	0.884	0.691	0.656	0.671
+TS	0.478 [1.30]	0.870 [1.03]	0.803 [1.38]	0.478 [1.31]	0.424 [1.29]	0.463 [1.30]
WRN	0.623	1.215	0.701	0.605	0.608	0.588
+TS	0.417 [1.33]	1.093 [0.97]	0.554 [1.37]	0.407 [1.33]	0.393 [1.33]	0.381 [1.34]
PreResNet56	0.639	0.799	0.881	0.606	0.586	0.628
+TS	0.462 [1.20]	0.634 [0.95]	0.729 [1.30]	0.424 [1.20]	0.428 [1.18]	0.444 [1.21]
CIFAR-100						
ResNet50	0.248	0.285	0.268	0.245	0.246	0.246
+TS	0.189 [1.36]	0.284 [1.02]	0.200 [1.37]	0.192 [1.36]	0.191 [1.30]	0.189 [1.36]
ResNet110	0.259	0.244	0.293	0.257	0.276	0.252
+TS	0.194 [1.36]	0.255 [1.07]	0.209 [1.38]	0.191 [1.36]	0.224 [1.27]	0.188 [1.36]
WRN	0.235	0.254	0.267	0.238	0.218	0.240
+TS	0.189 [1.37]	0.285 [1.09]	0.193 [1.38]	0.191 [1.36]	0.204 [1.35]	0.190 [1.36]
PreResNet56	0.271	0.271	0.308	0.264	0.223	0.265
+TS	0.228 [1.13]	0.273 [0.96]	0.255 [1.18]	0.220 [1.14]	0.196 [1.10]	0.221 [1.14]
Tiny-ImageNet						
ResNet50	0.127	0.177	0.136	0.127	0.122	0.123
+TS	0.152 [1.21]	0.195 [1.07]	0.160 [1.22]	0.153 [1.21]	0.139 [1.17]	0.151 [1.21]

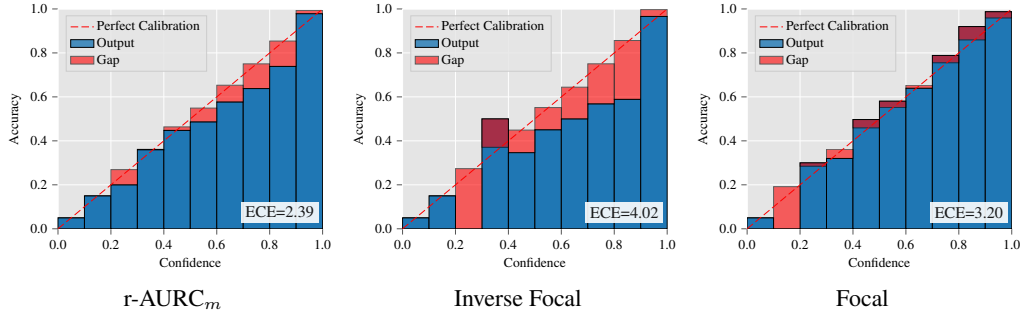


Figure 2: Reliability diagrams of PreResNet56 on CIFAR10. Top-label ECE reported at the bottom.

Regarding ECE, r-AURC achieves the best overall performance on CIFAR-10 across all architectures, and its ECE can likewise be improved through TS. Notably, focal loss performs relatively well in terms of ECE on CIFAR-100, suggesting its utility in top-label settings. Given that focal loss lacks a direct theoretical connection to calibration error minimization, we advocate for the use of inverse focal loss or r-AURC, both of which are explicitly designed to optimize calibration. Our r-AURC loss does not consistently achieve the lowest ECE across all datasets, suggesting a degree of dataset dependency or the need for incorporating a more reliable CSF to fully realize its calibration potential.

6 Conclusion and Limitation

In this work, we establish a theoretical connection between selective classification and calibration error minimization, and propose a differentiable loss function derived from the AURC metric. While this loss adopts a weighting scheme similar to that of inverse focal loss, it provides greater flexibility in the choice of CSFs, which contributes to its superior empirical performance. We introduce a general framework that enables the integration of this metric into a differentiable loss function using any CSF. A limitation of the r-AURC loss is that its performance depends on the quality of the chosen CSF. We therefore expect that incorporating more reliable confidence estimation methods will further improve the calibration performance of our approach.

Acknowledgement

This research received funding from the Flemish Government (AI Research Program) and the Research Foundation - Flanders (FWO) through project number G0G2921N. HZ is supported by the China Scholarship Council. We acknowledge EuroHPC JU for awarding the project ID EHPC-BEN-2025B22-061 and EHPC-BEN-2025B22-037 access to the EuroHPC supercomputer LEONARDO, hosted by CINECA (Italy) and the LEONARDO consortium.

References

- [1] Josh Achiam, Steven Adler, Sandhini Agarwal, Lama Ahmad, Ilge Akkaya, Florencia Leoni Aleman, Diogo Almeida, Janko Altenschmidt, Sam Altman, Shyamal Anadkat, et al. Gpt-4 technical report. *arXiv preprint arXiv:2303.08774*, 2023.
- [2] Mohamed Ishmael Belghazi and David Lopez-Paz. What classifiers know what they don't? *arXiv preprint arXiv:2107.06217*, 2021.
- [3] Mathieu Blondel, Olivier Teboul, Quentin Berthet, and Josip Djolonga. Fast differentiable sorting and ranking. In *International Conference on Machine Learning*, pages 950–959. PMLR, 2020.
- [4] Ondrej Bohdal, Yongxin Yang, and Timothy M Hospedales. Meta-calibration: Learning of model calibration using differentiable expected calibration error. *Transactions on Machine Learning Research*, pages 1–21, 2023.
- [5] Glenn W Brier. Verification of forecasts expressed in terms of probability. *Monthly weather review*, 78(1):1–3, 1950.
- [6] Nontawat Charoenphakdee, Jayakorn Vongkulbhaisal, Nuttapong Chairatanakul, and Masashi Sugiyama. On focal loss for class-posterior probability estimation: A theoretical perspective. In *Proceedings of the IEEE/CVF Conference on Computer Vision and Pattern Recognition*, pages 5202–5211, 2021.
- [7] Marco Cuturi, Olivier Teboul, and Jean-Philippe Vert. Differentiable ranking and sorting using optimal transport. *Advances in neural information processing systems*, 32, 2019.
- [8] Jia Deng, Wei Dong, Richard Socher, Li-Jia Li, Kai Li, and Li Fei-Fei. Imagenet: A large-scale hierarchical image database. In *2009 IEEE conference on computer vision and pattern recognition*, pages 248–255. Ieee, 2009.
- [9] Yukun Ding, Jinglan Liu, Jinjun Xiong, and Yiyu Shi. Revisiting the evaluation of uncertainty estimation and its application to explore model complexity-uncertainty trade-off. In *Proceedings of the IEEE/CVF Conference on Computer Vision and Pattern Recognition Workshops*, pages 4–5, 2020.
- [10] Zhipeng Ding, Xu Han, Peirong Liu, and Marc Niethammer. Local temperature scaling for probability calibration. In *Proceedings of the IEEE/CVF International Conference on Computer Vision*, pages 6889–6899, 2021.
- [11] Yasushi Esaki, Akihiro Nakamura, Keisuke Kawano, Ryoko Tokuhisa, and Takuro Kutsuna. Accuracy-preserving calibration via statistical modeling on probability simplex. In *International Conference on Artificial Intelligence and Statistics*, pages 1666–1674. PMLR, 2024.
- [12] Ido Galil, Mohammed Dabbah, and Ran El-Yaniv. What can we learn from the selective prediction and uncertainty estimation performance of 523 imagenet classifiers? In *The Eleventh International Conference on Learning Representations*, 2023.
- [13] Yonatan Geifman and Ran El-Yaniv. Selective classification for deep neural networks. *Advances in neural information processing systems*, 30, 2017.
- [14] Yonatan Geifman, Guy Uziel, and Ran El-Yaniv. Bias-reduced uncertainty estimation for deep neural classifiers. In *International Conference on Learning Representations*, 2019.

[15] Arindam Ghosh, Thomas Schaaf, and Matthew Gormley. Adafoocal: Calibration-aware adaptive focal loss. *Advances in Neural Information Processing Systems*, 35:1583–1595, 2022.

[16] Sebastian Gruber and Florian Buettner. Better uncertainty calibration via proper scores for classification and beyond. *Advances in Neural Information Processing Systems*, 35:8618–8632, 2022.

[17] Chuan Guo, Geoff Pleiss, Yu Sun, and Kilian Q Weinberger. On calibration of modern neural networks. In *International conference on machine learning*, pages 1321–1330. PMLR, 2017.

[18] Chirag Gupta and Aaditya Ramdas. Top-label calibration and multiclass-to-binary reductions. In *International Conference on Learning Representations*, 2022.

[19] Sarah Haggenmüller, Roman C Maron, Achim Hekler, Jochen S Utikal, Catarina Barata, Raymond L Barnhill, Helmut Beltraminelli, Carola Berking, Brigid Betz-Stablein, Andreas Blum, et al. Skin cancer classification via convolutional neural networks: systematic review of studies involving human experts. *European Journal of Cancer*, 156:202–216, 2021.

[20] Kaiming He, Xiangyu Zhang, Shaoqing Ren, and Jian Sun. Deep residual learning for image recognition. In *Proceedings of the IEEE conference on computer vision and pattern recognition*, pages 770–778, 2016.

[21] Kaiming He, Xiangyu Zhang, Shaoqing Ren, and Jian Sun. Identity mappings in deep residual networks. In *Computer Vision–ECCV 2016: 14th European Conference, Amsterdam, The Netherlands, October 11–14, 2016, Proceedings, Part IV 14*, pages 630–645. Springer, 2016.

[22] Dan Hendrycks and Kevin Gimpel. A baseline for detecting misclassified and out-of-distribution examples in neural networks. In *International Conference on Learning Representations*, 2022.

[23] L Hui. Evaluation of neural architectures trained with square loss vs cross-entropy in classification tasks. In *The Ninth International Conference on Learning Representations (ICLR 2021)*, 2020.

[24] Abhay Karandikar, Nicholas Cain, Dinh Tran, Balaji Lakshminarayanan, Jonathon Shlens, Michael C Mozer, and Rebecca Roelofs. Soft calibration objectives for neural networks. In *Advances in Neural Information Processing Systems*, volume 34, pages 29768–29779, 2021.

[25] Viacheslav Komisarenko and Meelis Kull. Improving calibration by relating focal loss, temperature scaling, and properness. In *ECAI 2024*, pages 1535–1542. IOS Press, 2024.

[26] Ramesh Krishnan and Omesh Tickoo. Improving model calibration with accuracy versus uncertainty optimization. In *Advances in Neural Information Processing Systems*, volume 33, pages 18237–18248, 2020.

[27] A Krizhevsky. Learning multiple layers of features from tiny images. *Master’s thesis, University of Tront*, 2009.

[28] Meelis Kull, Telmo Silva Filho, and Peter Flach. Beta calibration: a well-founded and easily implemented improvement on logistic calibration for binary classifiers. In *Artificial intelligence and statistics*, pages 623–631. PMLR, 2017.

[29] Meelis Kull, Miquel Perello Nieto, Markus Kängsepp, Telmo Silva Filho, Hao Song, and Peter Flach. Beyond temperature scaling: Obtaining well-calibrated multi-class probabilities with dirichlet calibration. *Advances in neural information processing systems*, 32, 2019.

[30] Ananya Kumar, Percy S Liang, and Tengyu Ma. Verified uncertainty calibration. *Advances in neural information processing systems*, 32, 2019.

[31] Aviral Kumar, Sunita Sarawagi, and Ujjwal Jain. Trainable calibration measures for neural networks from kernel mean embeddings. In *Proceedings of the 35th International Conference on Machine Learning*, pages 2805–2814. PMLR, 2018.

[32] Tsung-Yi Lin, Priya Goyal, Ross Girshick, Kaiming He, and Piotr Dollár. Focal loss for dense object detection. In *Proceedings of the IEEE international conference on computer vision*, pages 2980–2988, 2017.

[33] Aixin Liu, Bei Feng, Bing Xue, Bingxuan Wang, Bochao Wu, Chengda Lu, Chenggang Zhao, Chengqi Deng, Chenyu Zhang, Chong Ruan, et al. Deepseek-v3 technical report. *arXiv e-prints*, pages arXiv–2412, 2024.

[34] Weitang Liu, Xiaoyun Wang, John Owens, and Yixuan Li. Energy-based out-of-distribution detection. *Advances in neural information processing systems*, 33:21464–21475, 2020.

[35] Yuchi Liu, Lei Wang, Yuli Zou, James Zou, and Liang Zheng. Optimizing calibration by gaining aware of prediction correctness. *arXiv preprint arXiv:2404.13016*, 2024.

[36] Xingchen Ma and Matthew B. Blaschko. Meta-cal: Well-controlled post-hoc calibration by ranking. In *International Conference on Machine Learning*, 2021.

[37] Jishnu Mukhoti, Viveka Kulharia, Amartya Sanyal, Stuart Golodetz, Philip Torr, and Puneet Dokania. Calibrating deep neural networks using focal loss. *Advances in neural information processing systems*, 33:15288–15299, 2020.

[38] Michael Panchenko, Anes Benmerzoug, and Miguel de Benito Delgado. Class-wise and reduced calibration methods. In *2022 21st IEEE International Conference on Machine Learning and Applications (ICMLA)*, pages 1093–1100. IEEE, 2022.

[39] John Platt et al. Probabilistic outputs for support vector machines and comparisons to regularized likelihood methods. *Advances in large margin classifiers*, 10(3):61–74, 1999.

[40] Teodora Popordanoska, Raphael Sayer, and Matthew Blaschko. A consistent and differentiable l_p canonical calibration error estimator. *Advances in Neural Information Processing Systems*, 35:7933–7946, 2022.

[41] Linwei Tao, Minjing Dong, and Chang Xu. Dual focal loss for calibration. In *International Conference on Machine Learning*, pages 33833–33849. PMLR, 2023.

[42] Deng-Bao Wang, Lei Feng, and Min-Ling Zhang. Rethinking calibration of deep neural networks: Do not be afraid of overconfidence. *Advances in Neural Information Processing Systems*, 34:11809–11820, 2021.

[43] Jonathan Wenger, Hedvig Kjellström, and Rudolph Triebel. Non-parametric calibration for classification. In *International Conference on Artificial Intelligence and Statistics*, pages 178–190. PMLR, 2020.

[44] Ross Wightman. Pytorch image models. <https://github.com/rwightman/pytorch-image-models>, 2019.

[45] Sergey Zagoruyko and Nikos Komodakis. Wide residual networks. In *Proceedings of the British Machine Vision Conference 2016*, pages 87–1. British Machine Vision Association, 2016.

[46] Han Zhou, Jordy Van Landeghem, Teodora Popordanoska, and Matthew B. Blaschko. A novel characterization of the population area under the risk coverage curve (aurc) and rates of finite sample estimators. In *International Conference on Machine Learning*, 2025.

7 Appendix

7.1 Definitions

Definition 7.1 (Brier Score (BS)). The Brier Score of a model $f : \mathcal{X} \rightarrow \Delta^k$ is defined as:

$$\text{BS}(f) = \mathbb{E} [\|f(\mathbf{x}) - \mathbf{y}\|_2^2] \quad (23)$$

where $f(\mathbf{x})$ is the predicted probabilities and \mathbf{y} is the one-hot encoded label.

Confidence Score Functions (CSFs). The CSFs are generally defined as functions of the predicted probabilities \mathbf{p} , which are the outputs by passing the logits \mathbf{z} produced by the model for the input \mathbf{x} through the softmax function $\sigma(\cdot)$, expressed as $\mathbf{p} = \sigma(\mathbf{z}) \in \mathbb{R}^k$. The specific forms of these CSFs are outlined as follows:

Table 3: Commonly Used CSFs

Method	Equation
MSP	$g(\mathbf{p}) = \max_{i=1}^k p_i$
Softmax Margin	$g(\mathbf{p}) = p_i - \max_{j \neq i} p_j$ with $i = \arg \max_{i=1}^k p_i$
Negative Entropy	$g(\mathbf{p}) = \sum_{i=1}^k p_i \log p_i$

7.2 Proofs of Theoretical Results

Proof of Prop. 4.3. For any class-wise binning scheme $B = \{I_{c,b} \mid c = 1, \dots, k; b = 1, \dots, m_c\}$, let m_c be the number of bins for class c and $n_{c,b}$ be the number of samples falling into $I_{c,b}$, then by Minkowski inequality, we have

$$\widehat{\text{cwECE}}_B(f) = \frac{1}{k} \sum_{c=1}^k \frac{1}{n} \sum_{b=1}^{m_c} n_{c,b} \left| \underbrace{\frac{1}{n_{c,b}} \sum_{i \in I_{c,b}} \mathbb{I}(y'_i = c)}_{\text{acc}_{c,b}} - \underbrace{\frac{1}{n_{c,b}} \sum_{i \in I_{c,b}} f_c(\mathbf{x}_i)}_{\text{conf}_{c,b}} \right| \quad (24)$$

$$\leq \frac{1}{nk} \sum_{c=1}^k \sum_{b=1}^{m_c} \sum_{i \in I_{c,b}} \left| \mathbb{I}(y'_i = c) - f(\mathbf{x}_i)_c \right| \quad (25)$$

$$= \frac{1}{nk} \sum_{i=1}^n \sum_{c=1}^k \left| \mathbb{I}(y'_i = c) - f(\mathbf{x}_i)_c \right| \quad (26)$$

which implies $I_{c,b}$ can be further divided into $n_{c,b}$ sub-partitions so that each sub-partition contains exactly one sample. Let B^* denotes this implied binning scheme. Then we find the lower bound of $\widehat{\text{cwECE}}_{B^*}(f)$. For the wrongly classified sample in $I_{c,b}$ where the prediction $\hat{y}_i \neq y'_i$, we have

$$\sum_{c=1}^k \left| \mathbb{I}(y'_i = c) - f_c(\mathbf{x}_i) \right| = 2(1 - f_{y'_i}(\mathbf{x}_i)) > 1 \quad (27)$$

since only the true class contributes 1, $\sum_c f_c(\mathbf{x}_i) = 1$ and $f_{y'_i}(\mathbf{x}_i) < \frac{1}{2}$. For the correct classified sample in $I_{c,b}$, we have

$$\sum_{c=1}^k \left| \mathbb{I}(y'_i = c) - f_c(\mathbf{x}_i) \right| < 2(1 - \frac{1}{k}) \quad (28)$$

since $1 \geq f_{y'_i}(\mathbf{x}_i) > \frac{1}{k}$. Combine this equation with Eq. (26), then:

$$\sup_{B \in \mathcal{B}} \widehat{\text{cwECE}}_B(f) = \widehat{\text{cwECE}}_{B^*}(f) > \frac{1}{nk} \sum_{i=1}^n \mathbb{I}(\hat{y}_i \neq y'_i) = \frac{1}{k} \widehat{\text{err}}(f). \quad (29)$$

Then by applying Jensen's inequality, we obtain the first inequality in this proposition. \square

Proof of Prop. 4.7. Since g^* is perfectly aligned with the loss ℓ , by the definition of AURC, for any confidence map $g \in \mathcal{G}$, we have

$$\inf_{g \in \mathcal{G}} \widehat{\text{AURC}}_g(f) \geq \widehat{\text{AURC}}_{g^*}(f). \quad (30)$$

Using the inequality $-\ln(1-x) \geq x$ for $x \in (0, 1)$, we get:

$$\widehat{\text{AURC}}_{g^*}(f) = -\frac{1}{n} \sum_{i=1}^n \ln \left(1 - \frac{r_i}{n+1} \right) \ell(f(\mathbf{x}_i), \mathbf{y}_i) \geq \frac{1}{n(n+1)} \sum_{i=1}^n r_i \ell(f(\mathbf{x}_i), \mathbf{y}_i). \quad (31)$$

Let $\mathcal{E} := \{i : \hat{y}_i \neq y'_i\}$ be the set of misclassified samples, and let $n_1 = |\mathcal{E}| = n \cdot \widehat{\text{err}}(f)$. Since for incorrect predictions $f_{y'_i}(\mathbf{x}_i) < \frac{1}{2}$, the cross-entropy loss satisfies:

$$\ell(f(\mathbf{x}_i), \mathbf{y}_i) = -\log f_{y'_i}(\mathbf{x}_i) > \log 2 \quad \text{for all } i \in \mathcal{E}. \quad (32)$$

By the definition of g^* , the n_1 high-loss samples in \mathcal{E} must be assigned the smallest ranks $1, 2, \dots, n_1$. Therefore:

$$\sum_{i \in \mathcal{E}} r_i = 1 + 2 + \dots + n_1 = \frac{n_1(n_1+1)}{2}. \quad (33)$$

It follows that:

$$\widehat{\text{AURC}}_{g^*}(f) \geq \frac{1}{n(n+1)} \sum_{i \in \mathcal{E}} r_i \cdot \ell(f(\mathbf{x}_i), \mathbf{y}_i) > \frac{\log 2}{n(n+1)} \cdot \sum_{i \in \mathcal{E}} r_i = \frac{\log 2}{n(n+1)} \cdot \frac{n_1(n_1+1)}{2}. \quad (34)$$

Substitute $n_1 = n \cdot \widehat{\text{err}}(f)$, we obtain:

$$\widehat{\text{AURC}}_{g^*}(f) \geq \frac{\log 2}{2(n+1)} \cdot \widehat{\text{err}}(f) \cdot (n \cdot \widehat{\text{err}}(f) + 1) = \frac{n \log 2}{2(n+1)} \widehat{\text{err}}^2(f) + \frac{\log 2}{2(n+1)} \widehat{\text{err}}(f) \quad (35)$$

which completes the proof. \square

7.3 Gradient analysis

[Focal loss.] We consider the gradient of focal loss with respect to the true class predicted probability $p_{y'}$. By applying the product rule, we obtain:

$$\frac{\partial}{\partial p_{y'}} [-(1-p_{y'})^\gamma \log(p_{y'})] = \frac{\partial}{\partial p_{y'}} [-(1-p_{y'})^\gamma] \log(p_{y'}) + (1-p_{y'})^\gamma \frac{\partial}{\partial p_{y'}} \log(p_{y'}) \quad (36)$$

$$= \gamma(1-p_{y'})^{\gamma-1} \log(p_{y'}) - (1-p_{y'})^\gamma \frac{1}{p_{y'}}. \quad (37)$$

We can see that its gradient does shrink to 0 when $p_{y'} \rightarrow 1$ (see Fig. 3(a)).

[Inverse focal loss.] For inverse focal loss, similarly we can compute its gradient with respect to $p_{y'}$:

$$\frac{\partial}{\partial p_{y'}} [-(1+p_{y'})^\gamma \log(p_{y'})] = \frac{\partial}{\partial p_{y'}} [-(1+p_{y'})^\gamma] \log(p_{y'}) + (1+p_{y'})^\gamma \frac{\partial}{\partial p_{y'}} \log(p_{y'}) \quad (38)$$

$$= \gamma(1+p_{y'})^{\gamma-1} \log(p_{y'}) - (1+p_{y'})^\gamma \frac{1}{p_{y'}} \quad (39)$$

where we can see that its gradient does not shrink to 0 when $p_{y'} \rightarrow 1$ (see Fig. 3(b)). However, we notice that when γ is greater than 4, the gradient can be positive in some regions. In these cases, the inverse focal loss may not be suitable to optimize the model.

[AURC loss.] For AURC loss, we consider the gradient with respect to the weights. From the chain rule, we have

$$\frac{\partial [w(\mathbf{p})\ell(\mathbf{p}, \mathbf{y})]}{\partial \mathbf{p}} = w(\mathbf{p}) \frac{\partial \ell(\mathbf{p}, \mathbf{y})}{\partial \mathbf{p}} + \ell(\mathbf{p}, \mathbf{y}) \frac{\partial w(\mathbf{p})}{\partial \mathbf{p}}. \quad (40)$$

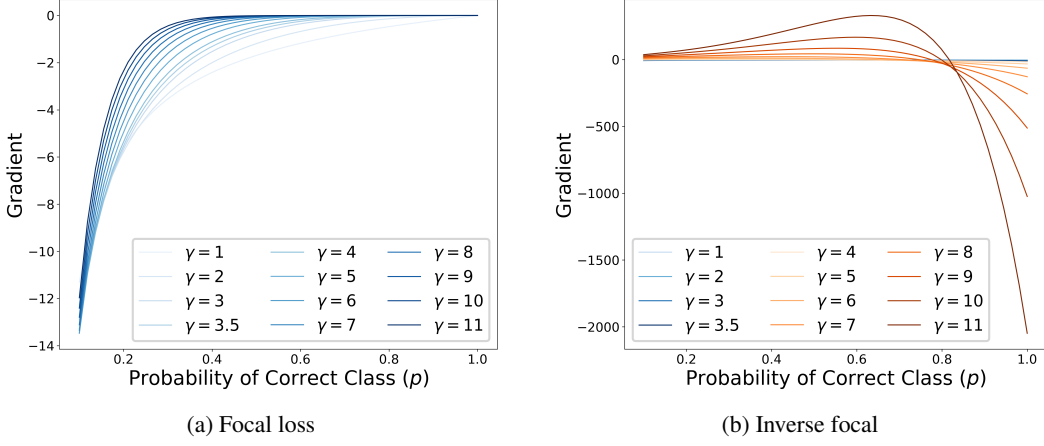


Figure 3: The gradient of loss ℓ with respect to $p_{y'}$

where $w(\mathbf{p}) = -\ln(1 - G(\mathbf{p}))$. Take ℓ as the cross-entropy loss, we consider the gradient of AURC with respect to $p_{y'}$:

$$\frac{\partial \ln(1 - G(\mathbf{p})) \ln(p_{y'})}{\partial p_{y'}} = [\ln(1 - G(\mathbf{p}))] \frac{\partial \ln(p_{y'})}{\partial p_{y'}} + \ln(p_{y'}) \frac{\partial [\ln(1 - G(\mathbf{p}))]}{\partial p_{y'}} \quad (41)$$

$$= \frac{[\ln(1 - G(\mathbf{p}))]}{p_{y'}} - \frac{\ln(p_{y'})}{1 - G(\mathbf{p})} \frac{\partial G(\mathbf{p})}{g(\mathbf{p})} \frac{\partial g(\mathbf{p})}{\partial p_{y'}} \quad (42)$$

since

$$\frac{\partial w(\mathbf{p})}{\partial p_{y'}} = \frac{\partial w(\mathbf{p})}{\partial G(\mathbf{p})} \cdot \frac{\partial G(\mathbf{p})}{\partial g(\mathbf{p})} \frac{\partial g(\mathbf{p})}{\partial p_{y'}} = \frac{1}{1 - G(\mathbf{p})} \cdot \frac{\partial G(\mathbf{p})}{\partial g(\mathbf{p})} \frac{\partial g(\mathbf{p})}{\partial p_{y'}}. \quad (43)$$

Since the value of $G(\cdot)$ can be approximated using the Monte Carlo method [46] as $\widehat{G(\mathbf{p})} = \frac{r(g(\mathbf{p}))}{n+1}$ where $r(g(\mathbf{p}))$ denotes the rank of $g(\mathbf{p})$ when the values are sorted in ascending order according to the CSF $g(\cdot)$. Following the soft ranking approach proposed by Blondel et al. [3], the hard (discrete) rank can be replaced with a differentiable soft rank $\hat{r}(g(\mathbf{p}))$ such that

$$\frac{\partial G(\mathbf{p})}{\partial g(\mathbf{p})} \approx \frac{\partial [\hat{r}(g(\mathbf{p}))/n+1]}{\partial g(\mathbf{p})}. \quad (44)$$

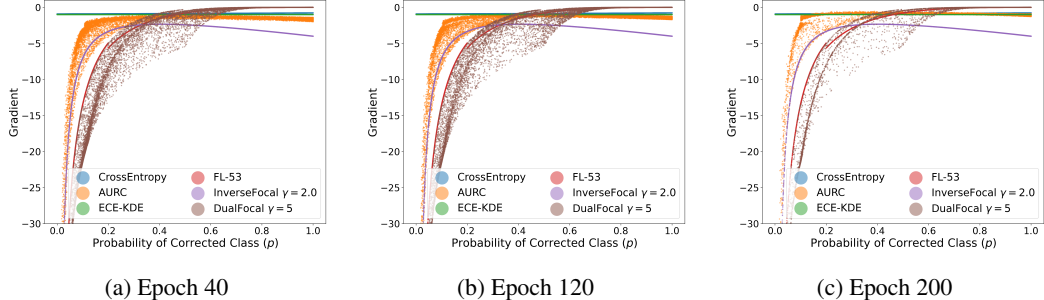


Figure 4: Evolution of the loss gradient $\frac{\partial \ell}{\partial p_{y'}}$ with respect to model prediction probability $p_{y'}$ for the same ResNet model evaluated on 20,000 CIFAR-10 training samples, throughout the training process. To clearly illustrate the behavior of the r-AURC loss, we set $\lambda = 1.0$.

7.4 Training details

The experiments are conducted using NVIDIA P100 GPUs. All models are trained using stochastic gradient descent (SGD) with a momentum of 0.9 and a mini-batch size of 128. We apply ℓ_2 weight

decay regularization term of 0.0005. Training is conducted for 200 epochs on CIFAR-10/100, and for 100 epochs on Tiny-ImageNet. For CIFAR-10 and CIFAR-100, the learning rate is initialized at 0.01 and reduced to 0.001 at epoch 150. For Tiny-ImageNet, the learning rate schedule is set to 0.01 initially, reduced to 0.001 at epoch 40, and further decreased to 0.0001 at epoch 60. For each loss function, we report the performance of the best model checkpoint selected based on the lowest ECE observed after 120 epochs for CIFAR10/100.

[Model selection.] For dual focal loss and inverse focal loss, We applied cross-validation to determine the appropriate value of γ , following the approach described in Mukhoti et al. [37], Tao et al. [41]. Specifically, we held out 5,000 images from the training set as a validation set, trained on those images, and evaluate performance on the test set to select the best γ for the minimum ECE values after enough training epoches. We list those selected γ values in Table 4. We also present the selection γ for inverse focal loss in Figure 5, which also illustrates that values of $\gamma \geq 4$ should not be considered for this loss function.

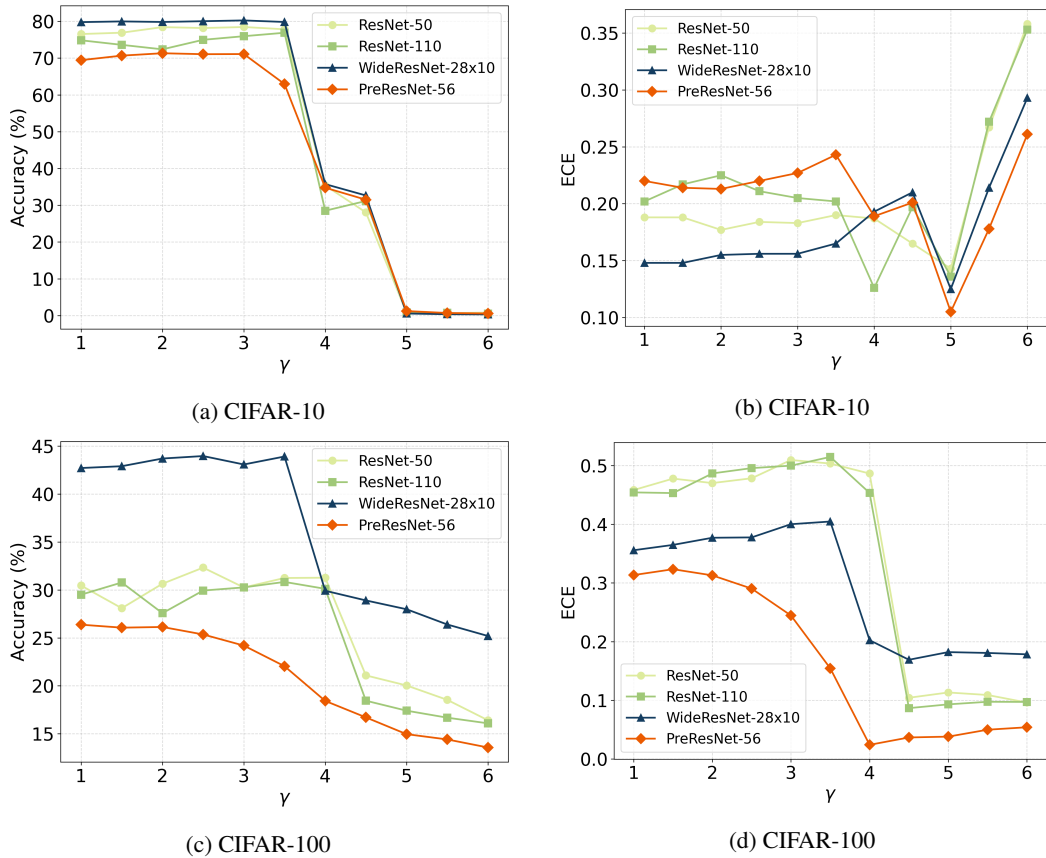


Figure 5: γ selection for inverse focal loss using cross-validation on CIFAR-10 and CIFAR-100 datasets.

Table 4: Selection of γ parameter for dual focal loss and inverse focal loss.

Dataset	CIFAR-10		CIFAR-100		Tiny ImageNet	
	Dual focal	Inv.FL	Dual focal	Inv.FL	Dual focal	Inv.FL
Architecture						
ResNet50	5.0	2.0	5.0	1.0	2.3	1.0
ResNet110	4.5	3.0	6.1	1.5	-	-
WRN	2.6	1.5	3.9	1.0	-	-
PreResNet56	4.0	2.0	4.5	1.0	-	-

7.5 Additional Experimental Results

We also report the training results of ECE as shown in Table 5. The r-AURC losses consistently achieve lower ECE compared to other baselines on CIFAR-10. On CIFAR-100, however, focal loss yields the best ECE performance, indicating that it may be effective in the top-label setting. For Tiny-ImageNet, FL-53 appears to be less reliable, showing degraded performance after TS. Overall, the results demonstrate that r-AURC is a strong candidate for improving calibration, both before and after TS/*MetaAcc*.

Table 5: Mean ECE $\times 10^2$ (\downarrow) before and after TS/*MetaAcc*. The temperature T selected by minimizing ECE on the training set is shown in brackets.

Model	XE	FL-53	Inv. FL	r-A _p	r-A _e	r-A _m
CIFAR-10						
ResNet50	2.89	3.60	3.75	2.82	2.81	2.91
+TS	1.84 [1.30]	4.00 [1.02]	3.14 [1.36]	1.76 [1.29]	1.60 [1.28]	1.84 [1.30]
+MetaAcc	0.36	3.58	0.75	0.31	0.19	0.22
ResNet110	3.04	3.14	4.22	3.16	2.97	3.04
+TS	1.99 [1.30]	3.74 [1.03]	3.79 [1.38]	2.00 [1.30]	1.70 [1.29]	1.87 [1.30]
+MetaAcc	0.33	3.58	0.75	0.41	0.18	0.32
WRN	2.78	4.65	3.21	2.65	2.72	2.58
+TS	1.71 [1.33]	3.85 [0.97]	2.41 [1.37]	1.48 [1.33]	1.41 [1.33]	1.35 [1.34]
+MetaAcc	0.24	4.07	0.59	0.48	0.55	0.29
PreResNet56	2.79	3.28	4.10	2.56	2.49	2.66
+TS	1.71 [1.20]	2.31 [0.94]	3.27 [1.30]	1.46 [1.20]	1.48 [1.18]	1.61 [1.21]
+MetaAcc	0.67	3.15	1.06	0.51	0.71	0.75
CIFAR-100						
ResNet50	9.65	1.15	10.65	9.26	8.91	9.42
+TS	3.69 [1.36]	0.84 [1.02]	5.03 [1.37]	3.60 [1.36]	3.74 [1.30]	3.55 [1.36]
+MetaAcc	0.72	0.91	0.92	0.65	1.31	0.67
ResNet110	10.07	1.15	12.22	10.05	9.80	9.67
+TS	4.15 [1.36]	2.28 [1.07]	6.32 [1.38]	3.96 [1.36]	4.54 [1.27]	3.84 [1.36]
+MetaAcc	0.82	2.00	1.03	0.64	2.12	0.60
WRN	8.93	1.02	10.73	9.07	7.54	9.03
+TS	3.21 [1.37]	3.74 [1.09]	4.68 [1.38]	3.07 [1.36]	3.09 [1.35]	3.17 [1.36]
+MetaAcc	0.59	2.11	0.83	0.42	0.27	0.54
PreResNet56	9.80	1.12	12.21	9.31	6.85	9.41
+TS	7.03 [1.13]	2.39 [0.96]	8.94 [1.18]	6.24 [1.14]	4.58 [1.10]	6.37 [1.14]
+MetaAcc	5.57	1.53	7.54	5.14	4.12	5.40
Tiny-ImageNet						
ResNet50	0.90	6.85	1.36	1.04	1.63	0.93
+TS	6.56 [1.21]	10.25 [1.07]	7.04 [1.22]	6.56 [1.21]	4.98 [1.17]	6.55 [1.21]
+MetaAcc	6.48	9.92	6.83	6.54	4.99	6.58

Table 6 and 7 provides a overview of the testing performance of different trainable calibration methods. Results show that the r-AURC-based methods generally perform comparably to or better than other baselines especially on cwECE, while Dual Focal Loss and KDE-XE demonstrate competitive results with respect to ECE and ℓ_1 ECE^{KDE}, respectively.

Table 8 shows that the performance of *MetaAcc* differs in the models and dataset. For CIFAR100, it generally improves cwECE in most cases, with r-AURC_p, r-AURC_e, and r-AURC_m exhibiting competitive calibration. However, on CIFAR-10, cwECE sometimes increases—particularly for FL-53—while on Tiny-ImageNet, MetaAcc offers limited benefit and can occasionally degrade calibration. This table also suggests a trade-off associated with MetaAcc: in some cases, especially on CIFAR-100, improvements in calibration are accompanied by reductions in accuracy, with declines over 30% observed for certain models. These findings suggest that although MetaAcc may enhance calibration, it often does so at the expense of predictive accuracy, which limits its practical value.

Table 6: Test accuracy (%) and classwise ECE^a (↓), reported as mean $\times 10^2$ over 5 seeds.

Model	Accuracy (%) ↑					cwECE ^a (↓)				
	Dual	KDE-XE	r-A _p	r-A _e	r-A _m	Dual	KDE-XE	r-A _p	r-A _e	r-A _m
CIFAR-10										
ResNet50	94.5	94.8	94.6	94.3	94.6	0.230	0.263	0.260	0.249	0.259
ResNet110	90.7	94.7	94.4	94.2	94.5	0.830	0.253	0.264	0.271	0.269
WRN	91.8	95.4	95.4	95.2	95.6	0.829	0.241	0.251	0.245	0.220
PreResNet56	87.1	93.6	93.4	93.2	93.4	1.386	0.325	0.324	0.323	0.313
CIFAR-100										
ResNet50	76.6	77.6	77.7	76.3	77.6	0.126	0.101	0.111	0.104	0.111
ResNet110	76.1	77.3	77.4	71.9	77.5	0.118	0.097	0.109	0.138	0.110
WRN	77.9	79.0	78.7	78.7	78.9	0.178	0.118	0.124	0.152	0.125
PreResNet56	72.0	72.3	72.4	72.5	72.3	0.096	0.103	0.097	0.086	0.098
Tiny-ImageNet										
ResNet50	77.9	81.5	82.1	82.5	82.3	0.091	0.056	0.059	0.061	0.054

Table 7: ECE (↓) and ECE^{KDE} (↓), reported as mean $\times 10^2$ over 5 seeds.

Model	ECE (↓)					ℓ_1 ECE ^{KDE} (↓)				
	Dual	KDE-XE	r-A _p	r-A _e	r-A _m	Dual	KDE-XE	r-A _p	r-A _e	r-A _m
CIFAR-10										
ResNet50	0.81	2.77	2.82	2.81	2.91	6.99	4.51	4.80	5.03	4.52
ResNet110	1.02	3.11	3.16	2.97	3.04	15.72	4.59	4.79	4.96	4.60
WRN	0.74	2.70	2.65	2.72	2.58	13.01	4.12	4.28	4.35	4.14
PreResNet56	0.78	2.73	2.56	2.49	2.66	21.37	6.09	6.39	6.70	6.17
CIFAR-100										
ResNet50	0.71	9.57	9.26	8.91	9.42	47.22	29.58	29.86	32.67	29.93
ResNet110	0.82	10.50	10.05	9.80	9.67	47.53	29.14	29.28	40.35	29.51
WRN	1.03	8.86	9.07	7.54	9.03	44.80	27.85	27.97	30.33	27.97
PreResNet56	2.17	9.93	9.31	6.85	9.41	51.18	38.04	38.67	42.16	38.76
Tiny-ImageNet										
ResNet50	1.40	1.09	1.04	1.63	0.93	53.67	44.22	42.53	42.04	42.30

7.6 Parameter selection for r-AURC loss

Tuning parameter for Softrank Algorithm. We applied the *SoftRank* algorithm with quadratic regularization, as proposed by Karandikar et al. [24], which includes a regularization strength parameter ε that controls the trade-off between approximating the original operator and ensuring ‘smoothness’. A larger value of ε makes the objective function easier to optimize but at the cost of departing from the hard ranking. For top-k classification, we found that applying a confidence function map and tuning ε is crucial for performance, as demonstrated in [7, 24].

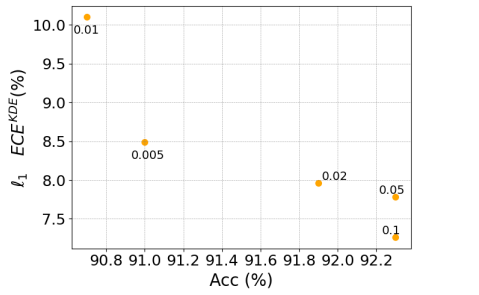
We report the testing performance of ResNet50 on the CIFAR-10 / 100 datasets in Table 9, and WideResNet-28x10 on the CIFAR-100 dataset in Table 10. As shown in these results, when the AURC dominates the loss function (i.e., $\lambda = 1$), the model performance becomes highly sensitive to the regularization parameter ε . This sensitivity is further illustrated by the comparison between Fig.6(a) and Fig.6(b).

Table 8: Mean cwECE $\times 10^2$ (\downarrow) before and after MetaAcc. Brackets show accuracy (%).

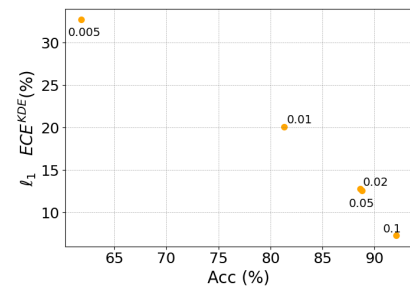
Model	XE	FL-53	Inv. FL	r-A _p	r-A _e	r-A _m
CIFAR-10						
ResNet50	0.64 [94.75]	0.84 [94.43]	0.81 [95.00]	0.63 [94.61]	0.62 [94.30]	0.64 [94.63]
+MetaAcc	0.67 [79.62]	1.06 [72.76]	0.61 [83.18]	0.72 [77.67]	0.71 [78.55]	0.65 [78.95]
ResNet110	0.67 [94.56]	0.77 [94.32]	0.88 [95.05]	0.69 [94.44]	0.66 [94.25]	0.67 [94.53]
+MetaAcc	0.68 [78.47]	1.08 [73.28]	0.70 [82.59]	0.69 [78.93]	0.72 [78.18]	0.69 [79.11]
WRN	0.62 [95.30]	1.21 [94.03]	0.70 [95.42]	0.60 [95.42]	0.61 [95.17]	0.59 [95.56]
+MetaAcc	0.71 [77.18]	1.60 [76.67]	0.72 [78.74]	0.78 [76.55]	0.74 [75.88]	0.89 [74.86]
PreResNet56	0.64 [93.39]	0.80 [93.05]	0.88 [93.78]	0.61 [93.36]	0.59 [93.22]	0.63 [93.38]
+MetaAcc	0.65 [82.68]	1.10 [74.16]	0.72 [79.92]	0.69 [80.31]	0.62 [82.85]	0.68 [82.24]
CIFAR-100						
ResNet50	0.25 [77.54]	0.29 [68.08]	0.27 [77.92]	0.25 [77.68]	0.25 [76.30]	0.25 [77.62]
+MetaAcc	0.13 [40.30]	0.28 [65.98]	0.13 [40.41]	0.13 [39.45]	0.15 [49.25]	0.13 [39.77]
ResNet110	0.26 [77.21]	0.24 [71.13]	0.29 [77.32]	0.26 [77.43]	0.28 [71.87]	0.25 [77.49]
+MetaAcc	0.13 [39.42]	0.24 [58.70]	0.13 [41.60]	0.13 [38.23]	0.19 [48.03]	0.13 [38.82]
WRN	0.24 [78.68]	0.25 [72.68]	0.27 [78.73]	0.24 [78.73]	0.22 [78.66]	0.24 [78.86]
+MetaAcc	0.13 [38.11]	0.23 [54.16]	0.14 [39.74]	0.14 [37.40]	0.13 [35.48]	0.14 [37.63]
PreResNet56	0.27 [72.21]	0.27 [66.06]	0.31 [72.63]	0.26 [72.43]	0.22 [72.53]	0.26 [72.34]
+MetaAcc	0.22 [68.71]	0.27 [56.51]	0.24 [69.75]	0.21 [69.97]	0.20 [71.62]	0.22 [69.77]
Tiny-ImageNet						
ResNet50	0.13 [81.84]	0.18 [78.24]	0.14 [79.56]	0.13 [82.11]	0.12 [82.47]	0.12 [82.31]
+MetaAcc	0.15 [80.71]	0.19 [74.96]	0.15 [76.63]	0.15 [81.17]	0.14 [81.74]	0.15 [81.37]

Table 9: Testing performance of ResNet50 on CIFAR-10/100 datasets using r-AURC_e loss under different λ and ε values. Except for AURC, all metrics are presented as values multiplied by 10^2 .

Dataset	ε	$\lambda = 0.5$					$\lambda = 1.0$						
		Acc	ℓ_1	ECE ^{KDE}	Brier	ECE	AURC	Acc	ℓ_1	ECE ^{KDE}	Brier	ECE	AURC
CIFAR-10	0.005	91.0	8.49	1.37	4.09	0.37	61.8	32.7	4.90	2.53	0.57		
	0.01	90.7	10.1	1.42	4.08	0.38	81.3	20.1	2.60	2.09	0.17		
	0.02	91.9	7.96	1.22	3.79	0.33	88.6	12.8	1.65	2.11	0.07		
	0.05	92.3	7.78	1.19	3.63	0.36	88.8	12.6	1.77	4.30	0.09		
	0.1	92.3	7.26	1.21	3.86	0.353	92.1	7.30	1.24	3.60	0.07		
CIFAR-100	0.005	64.2	50.1	0.50	13.2	1.50	25.2	142	0.89	11.6	3.31		
	0.01	71.2	37.2	0.42	12.7	1.43	50.8	90.7	0.61	5.05	1.64		
	0.02	71.5	37.0	0.41	12.6	1.42	50.7	87.0	0.63	7.88	1.75		
	0.05	70.0	39.9	0.44	12.7	1.43	68.7	57.6	0.43	7.23	0.91		
	0.1	70.1	38.7	0.44	14.5	1.58	70.6	39.8	0.43	12.9	1.34		



(a) $\lambda = 0.5$



(b) $\lambda = 1.0$

Figure 6: ℓ_1 ECE^{KDE} for top-label calibration using ResNet50 on CIFAR-10 test set.

Table 10: Testing performance of WideResNet-28x10 on CIFAR100 dataset when training with $r\text{-AURC}_e$ loss under different λ and ε values. Except for AURC, all metrics are presented as values multiplied by 10^2 ..

ε	$\lambda = 0.5$					$\lambda = 1$						
	Acc	ℓ_1	ECE^{KDE}	Brier	ECE	AURC	Acc	ℓ_1	ECE^{KDE}	Brier	ECE	AURC
0.005	60.6	60.2	0.53	11.8	1.35	36.1	115	0.75	4.15	2.07		
0.01	76.6	34.8	0.34	8.04	0.87	49.9	86.0	0.64	10.1	1.69		
0.02	72.5	41.1	0.39	9.51	1.11	56.0	73.5	0.57	9.39	1.37		
0.05	74.4	37.4	0.37	9.18	1.01	69.4	57.3	0.42	6.50	0.81		
0.1	72.9	40.4	0.38	9.26	1.06	76.4	37.0	0.340	7.15	0.81		

Ablation study on the trade-off parameter of the $r\text{-AURC}$ loss. For the λ parameter in Eq. (22) that controls the trade-off between AURC and cross-entropy loss, we investigate the effect of this parameter on the training process. We can see that for CIFAR10/100 dataset, choosing $\lambda = 0.5$ gives comparable performance on the ResNet50 and WideResNet-28x10 models.

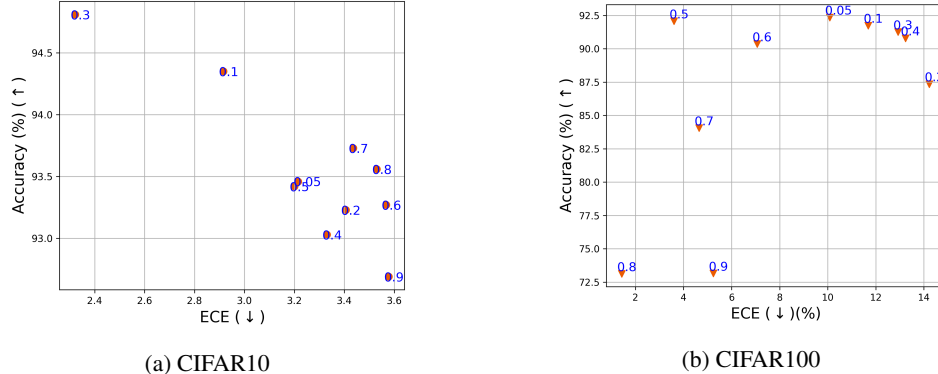


Figure 7: Testing performance of WideResNet-28x10 on the CIFAR-10/100, trained with $r\text{-AURC}_e$ loss, under varying values of λ . The regularization parameter is fixed to 0.05. We set the CSF function to be negative entropy for $r\text{-AURC}$ loss.

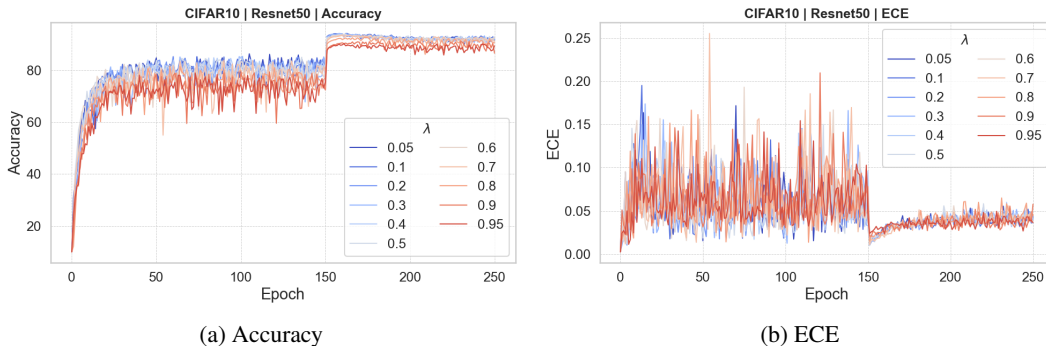


Figure 8: **(CIFAR10)** Evaluation metrics of **ResNet50** on the test set during training with $r\text{-AURC}$ loss while ε is fixed to be 0.05.